Landing Impact Protection through a Hybrid Attenuation System

E. J. MERZ,* J. A. BURNES,† AND S. R. MCCLURE‡
General Electric Company, Philadelphia, Pa.

A program to determine the most advantageous method of attenuating the landing shock of an unmanned system at terminal velocity of 20–200 fps with limited attitude control resulted in a hybrid pneumatic configuration having a hard-surfaced footpad on which a dual pneumatic bag attenuator is attached to support a payload cylinder. This approach is tolerant to impact attitude to 90° from flat, lateral velocity, surface slopes, and other uncertainties inherent in landing on unprepared surfaces. The concept can be applied to systems landing within the noted velocity range and results in deceleration levels on the payload of from 15 to over 200 g's. Seven drop tests of a 5-ft model have demonstrated the versatility of this configuration, the wide range of operating g levels and velocities, the close correlation of theory and test results, and the rebound limitation by spring-operated retraction reels.

Nomenclature

A = S_A/S_C
A_H = area of a crushable honeycomb impact attenuator
a = payload acceleration
E_g = work done by the lander against gravity (used in stability analysis)
E = energy absorbed in the crushable footpad assembly of the lander
G = deceleration at impact as a multiple of 32.2 ft/sec²
g = gravity constant for the planet indicated; on Earth g = 32.2 ft/sec².
H = height of a lander c.g. above a reference datum
h = free-fall height or engine burn out height
I = moment of inertia of arbor plus that of the belt wound on the arbor
I_0 = initial value of I
KE = kinetic energy
L = instantaneous radius of rotation of lander c.g. WR2 contact point
= length of belt from payload to skid
M = mass of the lander system
m_i = mass of ith body
m_a = mass of arbor
N_0 = initial number of turns of belt on arbor
N = number of turns rotated during impact
R = radius of lander footpad system
r = moment arm of belt to center of rotation of arbor
r_a = radius of arbor
S = stroke
S_A = actual geometric stroke of the impact system
S_c = stroke at impact based on a constant deceleration
t = thickness of crush-up material
t_b = belt thickness
T_0 = initial torque applied to the arbor by a spring
V = vertical impact velocity
V_0 = velocity at engine burnout for soft landers (taken positive downwards)
V_1 = velocity after impact
W = total weight of a lander
w = width of belt
α = angular acceleration of arbor
β = angle between belt and local vertical
σ = crushing stress phenolic honeycomb material
ρ = density of the melt material
θ,θ_1,θ_2 = angles used in defining impact touchdown condition (see Fig. 8)

Presented at the AIAA/ASME 11th Structures, Structural Dynamics, and Materials Conference, Denver, Colo., April 22–24, 1970 (no paper number; published in bound volume); submitted July 16, 1970; revision received November 9, 1970.

* Manager, Systems Development, Unmanned Systems, Space Systems Division. Member AIAA.
† Supervising Engineer, Structural Mechanics Laboratory, Re-entry and Environmental Systems Division. Member AIAA.
‡ Engineer, Systems Test Operation, Re-entry and Environmental Systems Division.

Introduction

THE design of systems to absorb the energy of impact and landing has classically proceeded from identification of a high-energy-absorption material to application of that material to the required payload configuration, and finally, resolution of stroke, g level, and weight factors based on impact velocity and attitude. In many cases, the limitations on materials properties or constraints on impact attitude or payload geometry have led to less than desirable combinations of stroke and deceleration g level. This is illustrated in Fig. 1 which presents the relative efficiency of various energy-absorbing materials and the impact pressure wherein they are effective. In Fig. 1, the pneumatic bag system has been normalized to an equivalent material basis as indicated for comparison with the competitive approaches.[1–5] The significant point of this presentation is that the pneumatic bag efficiency is independent of pressure, indicating freedom from the g-level constraint noted and results in maximum versatility; at the same time, the pneumatic bag is competitive on a weight basis with all other approaches in their best regimes. Although it has long been evident that pneumatic bags have this high potential, a specific configuration must be evolved for each application. In addition, some of the problems attendant to pneumatic attenuators[1,2,6] have deterred engineers from taking advantage of the inherent and often identified system advantages. Some of the most serious problems are: 1) the abrasion/puncture problem of fabric on unprepared surfaces; 2) the energy stored in the compressed gas which leads to rebound if not mitigaged; and 3) the instability of long-stroke pneumatic attenuators because of minimal shear and moment resistance in the pneumatic bags.

The hybrid pneumatic configuration described in this paper minimizes these disadvantages while retaining the advantages of pneumatic attenuators in coordination with other system requirements.

Problem Statement and Constraints

A system approach to definition of the most advantageous landing system for an unmanned planetary probe has led to the identification of a long stroke hybrid pneumatic energy attenuator as an outstanding candidate. The following requirements in the ranges noted[5] were used as technical ob-

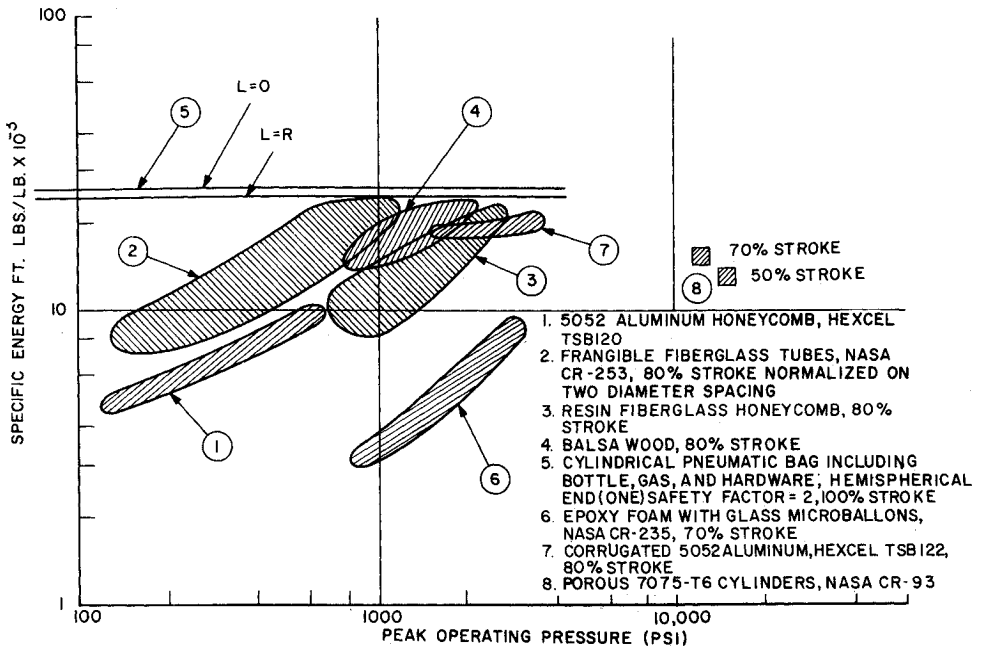

Fig. 1 Operating regime and efficiency of various impact limiter materials.

jectives in the study which resulted in the hybrid attenuator system described in the section on System Synthesis and Design: Impact velocity = 20–200 fps; Deceleration level = 20–500 Earth g's; Lateral velocity = 0–118 fps; Surface slopes = 0–20°; Vehicle attitude = ±40° at impact.

Although not all of the requirements in all combinations, particularly of impact velocity and g level, can be accommodated by a single design of realistic geometry, the configuration evolved can operate efficiently throughout the entire matrix. Figure 2 presents a nomograph relating the landing mechanics parameters involved and provides a means of visualizing, on one graph, the mechanics of motion of a landing vehicle from the time free-fall begins through the first impact stroke. Stability criteria for two specific hybrid lander configurations are plotted in the lower right-hand quadrant.

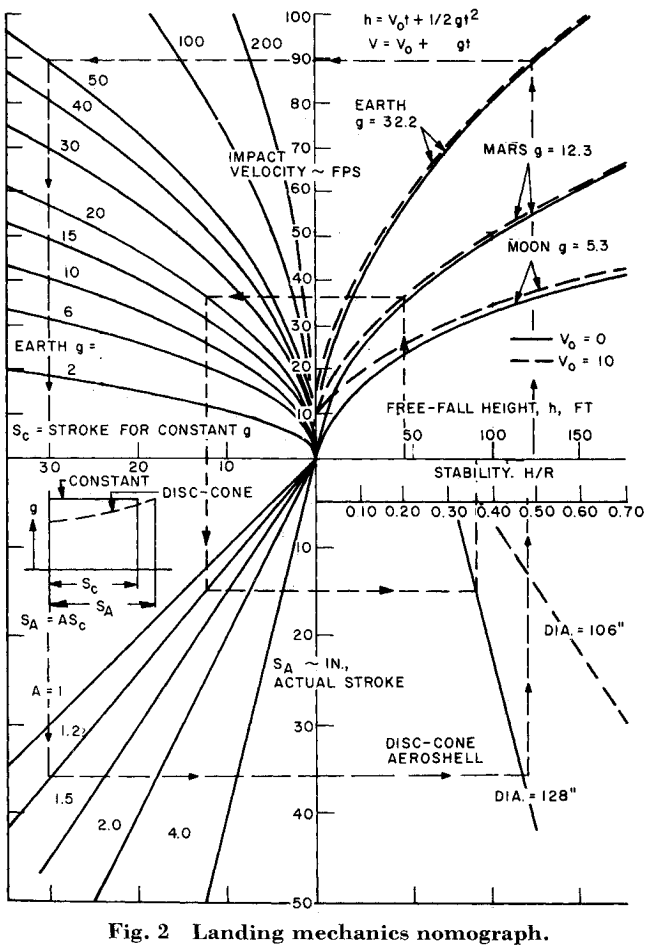

Fig. 2 Landing mechanics nomograph.

To use the nomograph, the upper right-hand quadrant is entered at the input free-fall height using the curve for the planet and V_0 selected. Reading impact velocity from this curve and extending the reference line horizontally to the desired value of impact deceleration of the payload, the stroke for constant deceleration may be read from the negative abscissa scale. Extending this point to the curve for A, the stroke-efficiency parameter, for the specific design being considered, determines the actual stroke. Carrying this value into the lower right-hand quadrant, the stability parameter H/R may be read for the aeroshell diameter of interest.

In summary, the nomograph uses simple mechanics to relate the various parameters but allows the systems analyst the choice of selecting parameters such as initial velocity and deceleration level, and also permits input of actual design values such as stroke efficiency and stability criteria for discrete designs. An important factor in the present system is its stroke efficiency that results in a near-square load-stroke curve as indicated in the inset of the lower left quadrant. This factor of $A = 1.2$ (in a vacuum) was a design objective and was achieved on the test model described in this paper. For vehicles landing on Earth, a factor of $A = 1.5$–2.0 is more realistic because of the one-atmosphere bias which must be added to initial gage pressure. Two examples are illustrated, one for an impact velocity of 36 fps, near maximum for a classical "soft" lander, and a second for an impact velocity of 90 fps, typical of a "rough" or "hard" lander.

System Synthesis and Design

The lander of Fig. 3 was derived from use of the aft portion of an entry aeroshell as a structural footpad to support and protect the pneumatic attenuator system, which in turn mitigates landing loads and shock imposed on the instrument payload. The model, approximately half-scale, shown in Fig. 3, was built and tested to demonstrate the concept. The payload container is supported on a cylindrical bag directly below it, which restrains upward travel at inflation and provides some shear restraint. The torus bag, attached to the top of the payload container provides lateral restraint at the

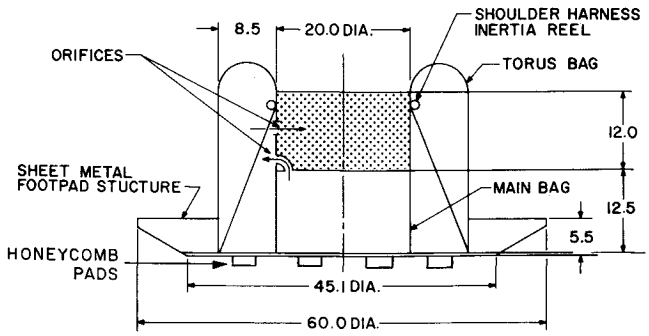

Fig. 3 Hybrid lander test model geometry; dimensions in inches.

top and greater volume in the bag system that limits both maximum pressure and pressure rise. Spring-actuated reels on the payload container wind up straps attached to the structural footpad and lock to prevent rebound. The fabric attenuator can be stowed (folded for minimum volume) and inflated a few minutes before impact. The payload container would be latched to the structural footpad and released at bag inflation. After impact the bags can be deflated slowly and the payload secured for instrument operation.

The hybrid lander is a system application of pneumatic attenuators and, as such, it is most realistically evaluated on a system basis. It is most efficient when the structural footpad is combined with or derived from a structure used for other purposes such as the entry aeroshell or launch vehicle adapter. The attractive system considerations are: 1) the long-stroke pneumatic attenuator; 2) the hard-surface footpad; 3) rebound limitation by the straps and reels; 4) the landing and landed stability; 5) the stroke efficiency attainable by shaping the bag; 6) the tolerance to off-nominal impact conditions including slopes, rocks, attitude and velocity; 7) the versatility of the system and flexibility in response to typical technical and program changes.

Theory and Analysis

The lander can be idealized as being comprised of two subsystems: the external shell and the pneumatic bag cavity (see Fig. 3). For purposes of initial exploratory studies, each subsystem was analyzed independently neglecting coupling effects to assess gross dynamic response. It must be emphasized that certain effects were not included in the analysis: elastic stretching of the pneumatic bag assembly, influence of reel loading on the payload container, stroke due to crushing of the honeycomb pads, real gas behavior, and strain energy in the footpad assembly. Most of the analysis presented was based on the half-scale model but applies equally to the generalized case with appropriate modifications of geometry and physical constants.

Analytical Model for the Pneumatic Bag Assembly

The analytical model used for the (nominal) closed pneumatic system is shown in Fig. 4. A computer program, which automates cross-sectional area computations and applies Simpson's Rule, when used in conjunction with the ideal gas laws, allows one to analyze closed pneumatic systems of rather arbitrary shape.

For closed pneumatic attenuation systems the ideal gas laws can be used within engineering accuracy. The adiabatic or isothermal processes are the most common. The difficulty that arises is that for complex shapes, or simple shapes being deformed in an arbitrary manner, the associated geometry is difficult to handle analytically. This problem is overcome by use of a code to approximate the system geometry and deformation characteristics. The code used in this study uses inputted strokes to compute areas which are then used in

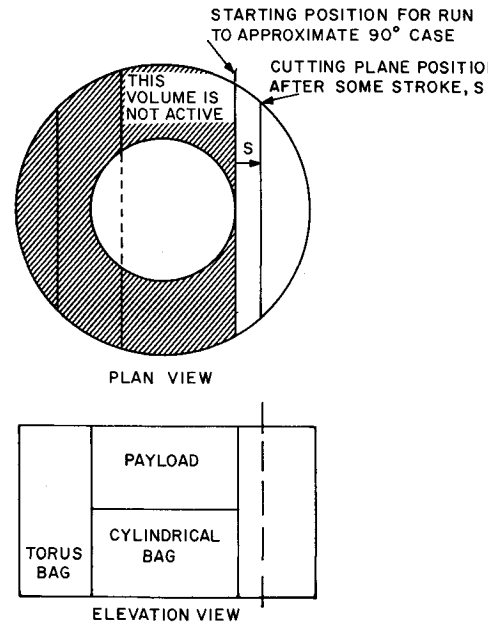

Fig. 4 Analytical model used for the direct approach to computing g loadings for closed pneumatic impact attenuation systems.

Simpson's Rule formulas to compute compressed volumes. The volumes and gas characteristics may then be related to rigid body g level developed in the system. One condition of interest for the Hybrid Lander is the dynamic loading on the payload container due to impact on a 20° slope with −24° attitude (see Fig. 5). The modeling of the problem is now summarized.

A computer run was processed for this case with the cutting plane positioned as indicated. Also, a simple fraction of the crushed area is used based upon the expected travel path of the payload. The area fraction was selected as follows. Engineering judgment and appeal to the geometry of the system indicated that for the 20° case, the actual effective area would be on the order of $\frac{1}{3}$ of the area found on a fully rigid crushing-plane basis. Although the actual model used was made up of two distinct bags, they were interconnected for purposes of this testing. It should also be noted that one basic a priori assumption is that the approximate motion is known in advance. Once the approximate planar (three-degree-of-freedom) motion is known, the associated travel can be inputted to the geometry/deformation computer program to determine the load stroke characteristics. Comparisons of the results of this approximate analysis technique to the dy-

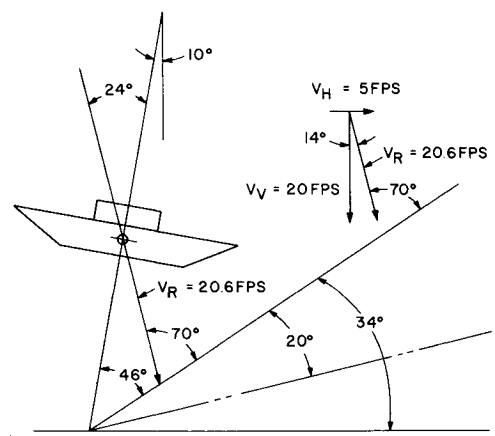

Fig. 5 Off nominal impact condition: touchdown on a 20° slope with adrene (−24°) attitude condition.

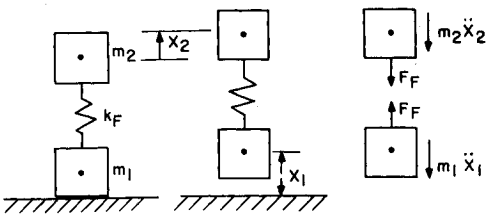

Fig. 6 Dynamic model used for analysis of bag fabric.

namic test data for the hybrid lander has shown that the method was accurate to within 10% in predicting peak g levels for the angular impact drop tests.

Bag Fabric Design

The bag fabric was specified through analysis of the loads introduced by internal pressure (initial and final) and the "snatch" loading produced at full impact stroke when the payload tends to move upward with respect to the base. The nominal pressure-produced fabric stresses were computed by application of thin shell formulas to the cylindrical and toroidal shapes. The dynamic snatch load was computed based on 60 fps relative velocity between the payload container and footpad structure. A simple model (single spring with two masses) (Fig. 6) was employed for the response calculations; it was further assumed that during the snatch a negligible pressure rise occurs. This analysis indicated the need for bag reinforcement in several areas to produce the desired safety margin.

Sheet Metal Footpad Structure

A dynamic load factor approach, based on worst case localized loading, was adopted to size the external sheet metal structure. The analysis consisted of determining the impact force transmitted through the special footpad assembly fixtures for angle drop tests and the several honeycomb pads for the (nominal) vertical drop tests.

Conventional stress analysis (using ample safety margins) was employed to size the sheet metal assembly, which in many aspects resembles an aeroshell class of structure. The material used was ductile Al alloy (6061-T6) in order to provide a capability for repetitive use of the model. An interesting feature of the footpad structure was that, by omission or inclusion of symmetric blocks of honeycomb base pads, various permutations in applied g levels were possible with use of a single honeycomb crush-up material. Since the boundary conditions allowed axial impact of the crushable phenolic honeycomb, direct mechanics relationships were applied to assess crush-up stroke and rigid body h level.[7,8] Thus, from Fig. 7 the relationship

$$\sigma A = WG$$

$$G = \sigma A/W$$

holds because of crushing force equivalence, where from energy transfer relationships

$$S = 0.5\ V^2/gG$$

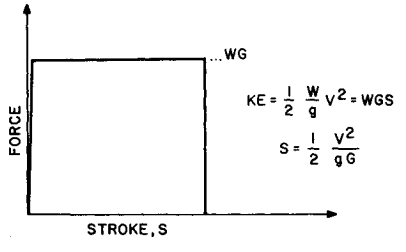

Fig. 7 Force vs stroke relationship for (ideal) crush-up system.

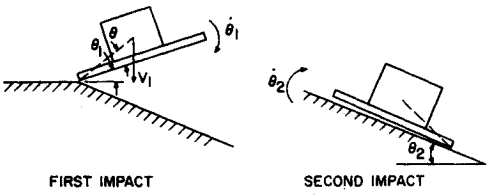

Fig. 8 Impact touchdown condition for stability studies.

Sufficient crush-up material thickness, ($t > S$) and appropriate g-level transducers[9] suited to a range of g's were specified via these equations. Some complexity was introduced by the angle-drop impact tests in that significant rotational motions were introduced. For these cases a three-degree-of-freedom dynamic response code was employed in the analysis to assure structurally adequate jig and fixturing for the test setup.

Dynamic Response Analysis of Inertia Reels

The reels used in the model consist of a coiled clock spring that serves to reel up the belt on an arbor and a ratchet to prevent unreeling or rebound by virtue of the stored energy in the bag systems. The torque applied by the clock spring produces an angular acceleration of the arbor after overcoming the inertia moments introduced by the acceleration of the extended portion of the belt. The two components of belt acceleration are the linear acceleration, $r\alpha$, and the in line component of the payload deceleration $a\cos\beta$. The appropriate equations of motion are

$$T = I\alpha + r(\rho whl)(r\alpha + a\cos\beta)$$

Here $\dot{I}$ is taken as small compared to I and w.

Moment of inertia I can be written approximately as

$$I = Mr_0^2/2 + 2\pi\rho wh(N_0 + n)[ra + 0.5(N_0 + n)h]^3$$

In practice, rather than measuring the thickness of the spooled belt, measurements of the extended length of the belt, and the moment arm of the belt to the center of rotation of the arbor were taken.

After substituting the particular reel geometry into the governing equation, a dimensionless relationship was established;

$$\frac{\alpha I_0}{T_0} = \frac{I/T_0 - 0.070\ ar_0(r)/T_0(r_0)}{I/I_0 + 0.070\ r_0^2r^2/I_0r_0}$$

Using typical spring torque profile data and an incremental calculation technique, the reel response time was computed. This was done to ensure that the reels would retract rapidly enough so that the rebound of the payload container would be effectively limited. The analytical data thus developed was used in a redesign of the reels to produce a travel time considerably lower than the payload stroke time of about 0.030 sec. The adequacy of the analysis and the hardware modifications was verified by the minimal rebound series of test drops.

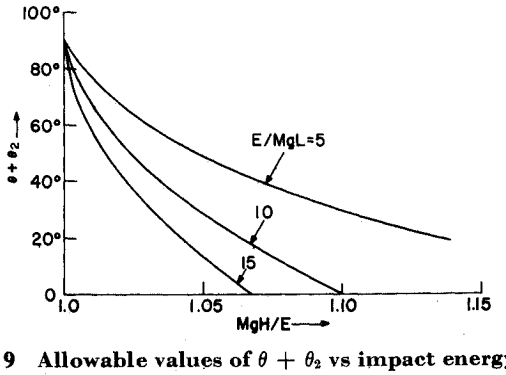

Fig. 9 Allowable values of $\theta + \theta_2$ vs impact energy, E.

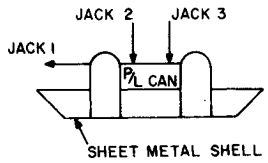

Fig. 10 Schematic of static test setup for the hybrid lander.

Stability

A first-order assessment was made of the stability of the hybrid configuration under nonideal impact conditions. The situation examined is shown in Fig. 8. In the analysis, the lander was modelled as a rigid body despite the fact that the payload and skid are separated by a soft-bag system and are of comparable mass.

First Impact

Assuming that there is no friction at the contact point, there will be no horizontal force developed and the c.g. will continue to move straight down after impact. If one equates initial kinetic energy, the initial conditions for the secondary impact may be established. Thus

$$V_1^2 = V_0^2/\{1 + [I/mL^2 \cos^2(\theta_1 + \theta)]\}$$

Second Impact

Assume that the crush-up footpad absorbs energy E during the second impact

$$mV_1^2 + I\theta_1^2 = mV_2^2 + I\theta_2^2 + 2E$$

where V_2 is the vertically upward bounce of the assembly after the second impact. Barring an excessive bounce, it is reasonable to assume that the edge of the assembly stays in contact with the plane, and

$$V_2 = \theta_2 L \cos(\theta_2 + \theta)$$

Toppling (instability) occurs when the c.g. moves clockwise above or slightly past the edge in contact with the plane. The work done against gravity is

$$E_g = ML[1 - \sin(\theta_2 + \theta)]g$$

Equating kinetic energy after the second impact with the work done against gravity,

$$0.5MV_2^2 + 0.5I\dot{\theta}_2 = E_g$$

Equating energies, combining terms, and introducing the free-fall height H corresponding to V_0 yields the constraint

$$\theta_2 + \theta = \sin^{-1}[1 - (H/L)(1 - E/MgH)]$$
$$= \sin^{-1}[1 - (E/MgL)(MgH/E - 1)]$$

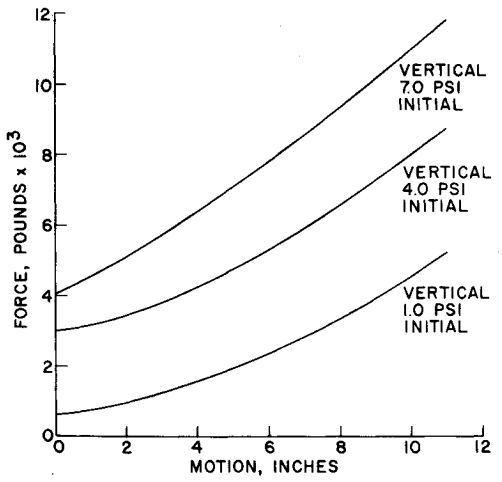

Fig. 11 Static test load/stroke data.

This relation is plotted as Fig. 9. The abscissa is the impact energy divided by the energy-absorbing capacity of the pad. Toppling occurs when this ratio exceeds unity. Although not fully investigated,[10,11] the test results lend credibility to this approximate analysis.

Experimental Program

The test program to confirm the performance of pneumatic attenuators consisted of two parts, the testing of a 69-in.-diam spherical model and the testing of the half-scale hybrid lander model. Because of concern about impact of fabric on rocks and unprepared surfaces, a long-stroke pneumatic configuration-simulation model was designed, built, and tested. The model consisted of two hemispheres of dacron fabric clamped to a built-up aluminum equatorial frame. The hemispheres were constructed of 8.8 oz/yd² dacron coated with 9.2 oz/yd² of polyurethane. The proof pressure was 6 psig, limit (at factor of 3) was 8.5 and burst 25.5 psig. The objectives of the tests were to test long-stroke attenuators characteristic of full size system configurations and to determine the effects on the fabric of impact on smooth rocks and slopes with lateral velocity.

The model was dropped on a flat surface at velocities increasing up to 60 fps and weights to 300 lb, then on a 10-in.-high cone simulating a smooth rock. It was then dropped on a smooth 45° ramp and finally on the 45° ramp having a 3-in.-high rock. This test simulated landing on a steep slope or with a severe lateral velocity and with rocks. All of the test parameters were close to those predicted and the model sus-

Table 1 69-in.-diam pneumatic model test summary

Test No.	2	3	4	5	7	8	9	10	12	13
Height	30 ft	40 ft	60 ft	75 ft	75 ft	85 ft	85 ft	85 ft	85 ft	85 ft
Surface	Flat	Flat	Flat	Flat	Flat 10-in. rock	Flat 10-in. rock	Flat	Flat	45° Flat	45°, 3-in. rock
Weight, lb	170	170	170	170	170	170	170	300	293	300
Imp. vel., fps	38.7	38.5	50.6	53.9	53.9	51.6	56.0	60.2	64.8	65.6
Rebound, ft	30.6	31.0	41.3	46.9	47.4	47.9	47.5	49.0		
Stroke, in.	21	21	25	23.4	24	23.4	23.4	26	13	16.4[a]
Pressure init., psig	0.93	0.93	0.93	0.93	1	1.03	1.12	1.03	2.02	1.99
Press. peak	3.3	3.4	5.6	6.33	6.34	5.88	5.66	9.7	5.	6.4
Peak g's	65.7	59.5	109.0	87.9	97.6	95.6	101.8	99.0	52.9[b] 68.8	40.7 39.9

[a] Measured from rock tip.
[b] Parallel to 45 surface.

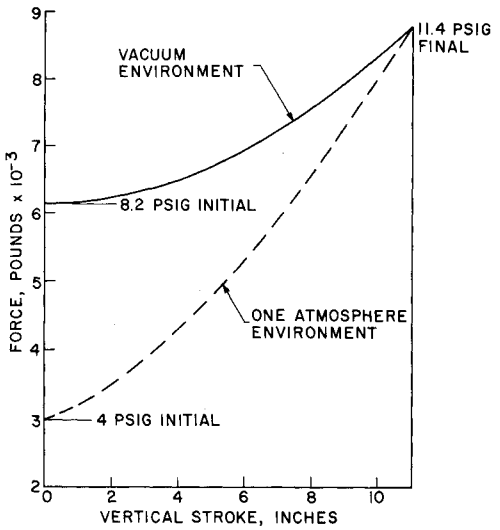

Fig. 12 Load stroke relations for vacuum and 1 atm.

tained no serious damage during the tests. A minor dimpling of the fabric surface was evident after dropping the 10-in. rock but this disappeared in a few days indicating complete recovery of the dacron fabric. A summary of the test results is given in Table 1.

As a result of these tests, design confidence was established for impact of fabric attenuators on smooth rocks, slopes to 45°, and slopes with rocks. Since the same model was used repeatedly on the rock tests and impacted at the same location, repeated impact on rocks at the same fabric location has been demonstrated. This series of tests, together with the abrasion resistance of the hard-surfaced footpad of the lander, have demonstrated effectively that puncture of pneumatic attenuators can be prevented by adequate design and testing.

Hybrid Lander Tests

The hybrid lander test series was designed to demonstrate the concept through several regimes of potential application. Specific test objectives included demonstration of the long-stroke (12 in. on half-scale model), high-impact velocity, impact angles to 90°, and the use of spring-operated reels in minimizing rebound. In order to obtain meaningful strokes in each test, the payload weight was changed inversely with impact velocity leading to a corresponding change in deceleration experienced at impact. Seven tests were made on the same model which was designed to be reusable for reasons of economy. The tests at angles of up to 90° were planned to demonstrate the adequacy of the configuration under adverse combinations of impact attitude and surface slope, and, thereby, to illustrate the tolerance of the configuration to off-nominal impacts.

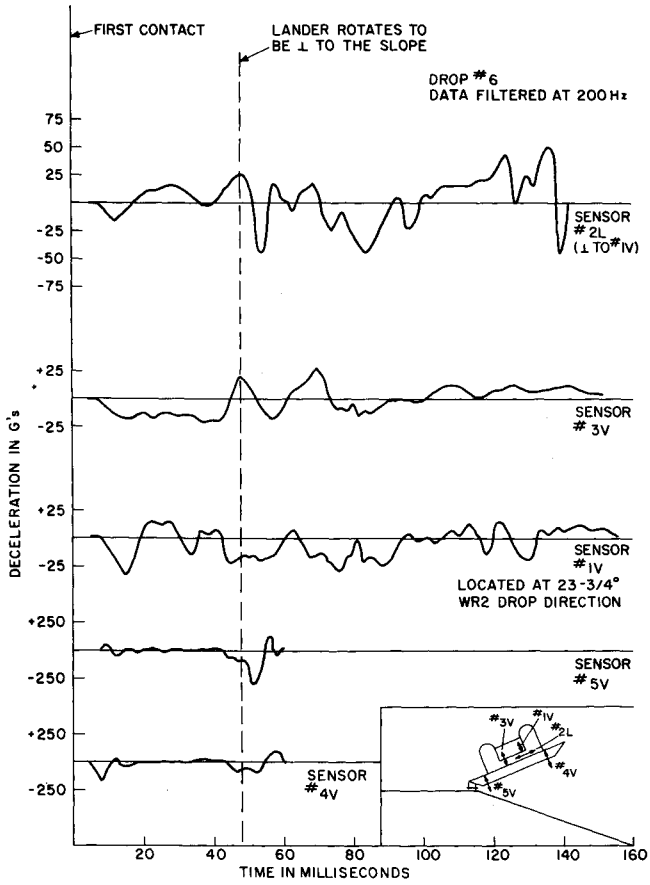

Fig. 13 Representative trace for lander impact upon a slope.

Static Tests

A valid stiffness matrix is needed as a prerequisite for more elaborate dynamic response studies. One way of obtaining the appropriate force displacement coefficients (and a bound on system performance) is via experimentation. For the study of this paper, a static test load-deflection program was used to determine stiffness characteristics of the complex pneumatic system. The test setup is shown schematically in Fig. 10. The applied loads were developed through a system of three hydraulic jacks, one lateral and two vertical. The measured deformations were taken along the (programed) direction of travel. An example of the data generated is given in Fig. 11. These results are for three initial pressures for a vertical load case with no tilt of the payload container. For a more complex case of angular loading, curves for vertical, lateral, and moment loading for various payload-tilt angles were also developed.

Using the static test data it is possible to develop the load-stroke characteristic curves for both vacuum and one-atmosphere ambient conditions in Fig. 12. If the pneumatic

Table 2 Hybrid lander test results

Drop	1	2	3	4	5	6	7
Attitude	Flat	Flat	6°	90°	22½°	23¼°	Flat
Height, ft	6.2	35	65	11.5	6.5	30	65
P/L weight, lb	215	107	85	107	210	105	85
Impact velocity, fps	19.2	42.2	51.5	26.5	20.4	41.2	57.4
Initial pressure, psig	2	2.4	5.9	1.9	2	4	6.1
Peak pressure, psig	5.8	9.8	11.8	4	5.4	7.3	12.1
Payload (Earth g's) deceleration	19	65	100	34	17	50	88
Footpad (Earth g's) deceleration	~500	~500	~400	~300	~100 ~200	~200 ~250	~800
Stroke, in.	7.6	8.9	7.1	6.4	6	7	8.1

Table 3 Comparison of test to predicted parameters

Drop number		1	2	3	4	5	6	7
Peak pressures, psig	Actual	5.8	9.8	11.8	4	5.4	7.3	12.1
	Theoretical	6	8.3	13.3	6.1	8	10	13.3
Peak g's on P/L (initial)	Actual	19	65	100	34	17	50	88
	Theoretical	19	55	110	33	15	55	110
P/L stroke	Actual	7.6	8.9	7.1	6.4	6	7	8.1
	Theoretical	7.5	10	10	8	<9.5	<9.5	10

system were to be deployed in a near-vacuum environment, the load-stroke curve would become more nearly rectangular, as indicated, which increases the stroke efficiency of the system. The curve shown for a vacuum has a stroke factor of 1.2 (length of stroke divided by the length of stroke for a constant load of the same magnitude).

Instrumentation

A variety of instrumentation was used to record and document the dynamic behavior of the hybrid lander during the drop test program. Although several permutations of instruments and locations were used, the fundamental data is comprised of: pressure readings (by transducers and Bourdon gages), accelerometer traces (using both crystal and strain gage models), and displacement measurements (by photonic sensors, scratch gages and reference markers). In addition, controlled sequences of motion picture films were also taken. The underlying philosophy of the test-data collection slan was to allow for redundancy and internal self-checking of the results. Representative traces for accelerometer locations are given in Fig. 13 for two points on the footpad assembly, two vertical and one lateral on the payload container.

Comparison of Theory to Test Results

Presented below are two tables which contain the summary of the hybrid lander test results. Table 2 contains the variable parameters and the test results for each drop test. Table 3 contains a comparison of actual vs theoretical or predicted peak pressure, peak g's on P/L, and P/L stroke. This latter table shows that there was a close correspondence between the actual and predicted values of the key parameters of internal pressure, stroke, and peak g loadings. The rebound was limited to less than a foot for the worst cases of vertical drops (from 65 ft). This indicates the energy of impact was effectively restrained by the strap and reel system. The capability of the model to adequately absorb impacts at up to 90° angles shows the shear capability of the attenuator and the general stability of the total configuration.

Conclusions

The experimental program produced test results in close agreement with theory with respect to pressure, stroke, and g-level parameters and, therefore, gives strong confidence in the analytical predictions. Verification was obtained for the capability of the hybrid configuration to mitigate three of the major problems of pneumatic attenuators; i.e., abrasion or rock puncture, rebound due to stored energy, and unidirectionality or instability. The hard surface footpad solves the abrasion problem and contributes to solution of the other two. The spring-operated straps and reels minimize rebound and the dual-bag system with the internal straps provides stability on the footpad structure and tolerance to impact over a wide range of impact angles.

The tests demonstrated impacts at 6°, 24°, and 90° as well as flat, which appears to be critical for stroke and peak g level. Reusability of the model and testing in a wide range of impact velocities (20–58 fps) was shown to be practical. As a result of the test series, it is possible to apply the configuration to landers in the soft, intermediate, and hard landing regimes.

References

[1] McGehee, J. R., "Investigation of a Compartmented Gas Bag Landing System Having Multiple Impact Capabilities," TN D-4710, 1968, NASA.

[2] McGehee, J. R., "Gas Bag Concept for a Storable Omnidirectional, Multiple Impact Landing System," *Journal of Spacecraft and Rockets*, Vol. 4, No. 10, Oct. 1967, pp. 1359–1362.

[3] Bresie, D., "Practical Limits for Balsa Impact Limiters," S-67-7287, 1966, NASA.

[4] Cloutier, G. J., "Crushable Material Energy Absorbers at Very High Impact Velocities," *Journal of Spacecraft and Rockets*, Vol. 3, No. 4, April 1966, p. 605.

[5] "Titan/Mars Hard Lander," NASA CR-66727, No. 1–8, Jan. 1969, Re-entry and Environmental Systems Div., General Electric Co.

[6] McGehee, J. R. and Hathaway, M. E., "Analytical Investigation of an Inflatable Landing System Having Omnidirectional and Multiple-Impact Capabilities," TN D5236, May 1969, NASA.

[7] Knoell, A. C., "Structural Development of an Impact Limiter System for a Mars Landing Vehicle," AIAA Paper 68-961, El Centro, Calif., 1968.

[8] Cundall, D. R., "Balsa Wood Impact Limiters for Hard Landing on the Surface of Mars," *AIAA/AAS Stepping Stones to Mars Meeting*, AIAA, New York, 1966, pp. 302–308.

[9] Levy, S. and Knoll, W., "Response of Accelerometer to Transient Accelerations," *Journal of Research of the Natural Bureau of Standards*, Vol. 45, No. 4, Oct. 1950, pp. 303 ff.

[10] Lavender, R. E., "On Touchdown Dynamics Analysis for Lunar Landing," *Proceedings of AIAA Symposium on Structural Dynamics and Aeroelasticity*, Boston, Mass., Aug. 30–Sept. 1, 1965, pp. 239–244.

[11] Jones, R. H. and Hinchey, S. D., "Some Basic Guidelines for Establishing Structural Design Parameters for the Landing Gear of Stable, Soft-Landing Spacecraft," AIAA Paper 68-345, Palm Springs, Calif., 1968.